AIAA JOURNAL
Vol. 41, No. 12, December 2003

Optimal Disturbances in Compressible Boundary Layers

Anatoli Tumin*
University of Arizona, Tucson, Arizona 85721
and
Eli Reshotko†
Case Western Reserve University, Cleveland, Ohio 44106

The problem of transient growth in compressible boundary layers is considered within the scope of partial differential equations including the nonparallel flow effects. As follows from previous investigations, the optimal disturbances correspond to steady counter-rotating streamwise vortices. The corresponding scaling of the perturbations leads to the governing equations for a Görtler-type of instability, with the Görtler number equal to zero. The iteration procedure employs back and forth marching solutions of the adjoint and original systems of equations. At low Mach numbers, the results agree with those for Blasius boundary-layer flows. In the case of parallel flows, the method leads to the same results obtained for compressible flows within the scope of linearized Navier–Stokes equations. It is shown that there is an optimal spacing of the streamwise vortices and an optimal location for their excitation.

Nomenclature

$\boldsymbol{A}, \boldsymbol{B}, \boldsymbol{D}$	=	matrices (5×5)
E	=	energy of the perturbation
G	=	energy ratio parameter in the present method
G^*	=	energy ratio parameter used in the case of parallel flow approximation
i	=	$\sqrt{-1}$
M	=	Mach number
Pr	=	Prandtl number
p	=	pressure
Re	=	Reynolds number, $\rho_\infty U_\infty L/\mu_\infty$
T	=	temperature
T_0	=	stagnation temperature
U	=	streamwise velocity component
u	=	streamwise velocity disturbance
V	=	normal velocity component
v	=	transverse velocity disturbance
w	=	spanwise velocity disturbance
x	=	streamwise coordinate
y	=	distance from the wall
z	=	spanwise coordinate
β	=	spanwise wave number
γ	=	specific heat ratio
θ	=	temperature disturbance
μ	=	viscosity
π	=	pressure disturbance
ρ	=	density

Subscripts

aw	=	adiabatic wall condition
in	=	input value
out	=	output value
s	=	base flow parameter
w	=	wall condition

Superscript

T	=	transposed

Presented as Paper 2003-0792 at the 41st Aerospace Sciences Meeting, Reno, NV, 6–9 January 2003; received 16 January 2003; revision received 31 July 2003; accepted for publication 31 July 2003.

*Associate Professor, Department of Aerospace and Mechanical Engineering. Senior Member AIAA.

†Kent H. Smith Professor Emeritus of Engineering, Department of Mechanical and Aerospace Engineering. Fellow AIAA.

Introduction

THE problem of optimal disturbances, in the context of bypass transition to turbulence, has been of great interest during the last decade. There are many applications where transition to turbulence occurs without exponentially growing (modal growth) disturbances such as Tollmien–Schlichting waves (see Ref. 1). According to theoretical and experimental data, there is a great potential for transient growth of the disturbance energy, even if the flow is stable with respect to wavelike perturbations. One can find a vast bibliography on the problem in the monograph by Schmid and Henningson.[2]

Transient growth arises from the coupling of slightly damped, highly oblique (nearly streamwise) Orr–Sommerfeld and Squire modes (see Ref. 2). The essence of the coupling is the following. The linearized Navier–Stokes equations for three-dimensional perturbations are reduced to a system of ordinary differential equations for the amplitude functions assuming that the solutions have a wavelike form. The equations can be recast as the Orr–Sommerfeld equation for the normal velocity component v and the equation for the normal vorticity. Specific to the normal vorticity equation is that it is driven by v, that is, the equation is coupled with the Orr–Sommerfeld equation. This coupling leads to algebraic growth, followed by exponential decay for the normal vorticity, although the solution for the normal velocity exponentially decays.[2]

Recently, the authors verified the potential importance of transient growth in explaining the long-standing blunt-body paradox[3] and the role of transient growth in Poiseuille pipe flow (see Ref. 4) and boundary-layer flow.[5] These three studies were the first to use a spatial growth formulation of these transient growth problems rather than the temporal growth approach.[6]

Temporal[6] and spatial[3,5] analyses of transient growth phenomenon in compressible boundary layers have been carried out within the scope of the parallel flow approximation, leading to questions about consistent comparison of theoretical and experimental data. Nonparallel flow effects were incorporated into the transient growth theory within the scope of linearized boundary-layer equations for the case of Blasius boundary-layer flow by Andersson et al.[7] and Luchini.[8] A compressible counterpart of this model has not yet been developed.

The objective of the present work is to develop a model of transient growth phenomena in compressible boundary layers that includes nonparallel flow effects.

Governing Equations

We consider steady three-dimensional disturbances in a compressible boundary layer over a flat plate. The characteristic length along the plate is L. We define a small parameter $\varepsilon = Re^{-1/2} = \sqrt{(\mu_\infty/\rho_\infty U_\infty L)}$, where U is the x-velocity component and the subscript ∞ stands for freestream parameters. The streamwise coordinate is scaled with L, whereas the vertical coordinate y and spanwise coordinate w are scaled with $\varepsilon L = \sqrt{(\mu_\infty L/\rho_\infty U_\infty)}$. The following scaling is assumed for the velocity disturbances u, v, and w; density ρ; pressure π; and temperature θ:

$$u \sim U_\infty, \qquad v \sim \varepsilon U_\infty, \qquad w \sim \varepsilon U_\infty$$
$$\rho \sim \rho_\infty, \qquad \pi \sim \varepsilon^2 \rho_\infty U_\infty^2, \qquad \theta \sim T_\infty \tag{1}$$

This scaling of the linearized Navier–Stokes equations leads to the governing equations for Görtler instability in a compressible boundary layer, with the Görtler number equal to zero (see Ref. 9). The perfect gas is characterized by the specific heat ratio $\gamma = 1.4$, the Prandtl number $Pr = 0.7$, and viscosity is considered as a function of the temperature in accordance with the Sutherland law. In what follows, the stagnation temperature T_0 is assumed equal to 333 K. Using the equation of state eliminates the density disturbance. We look for a periodic solution in the spanwise direction, that is, as an amplitude function of x and y times $\exp(i\beta z)$, with the corresponding wave number β. The following boundary conditions are applied to the solutions:

$$y = 0: u = v = w = \theta = 0, \qquad y \to \infty: u, w, \pi, \theta \to 0 \tag{2}$$

We introduce the vector-function $\boldsymbol{f}(x, y) = (u, v, w, \theta, \pi)^T$, where $w(x, y)$ is redefined as the amplitude function of the spanwise velocity component times i. The latter leads to the governing equations with real coefficients in the following form:

$$(\boldsymbol{A}\boldsymbol{f})_x = (\boldsymbol{D}\boldsymbol{f}_y)_x + \boldsymbol{B}_0\boldsymbol{f} + \boldsymbol{B}_1\boldsymbol{f}_y + \boldsymbol{B}_2\boldsymbol{f}_{yy} \tag{3}$$

where $\boldsymbol{A}, \boldsymbol{B}_0, \boldsymbol{B}_1, \boldsymbol{B}_2$, and $\boldsymbol{D}$ are 5×5 matrices. (Their nonzero elements are presented in Appendix A.) The matrix $\boldsymbol{D}$ has only one nonzero component, associated with $\partial^2 u/\partial x \partial y$, in the y-momentum equation. This term originated from the viscous terms of the equation. Numerical tests up to Mach 3 have shown that the term can be neglected for the optimal energy growth within an accuracy of 1%. The system of Eqs. (3) is parabolic in nature and can be solved by means of a downstream marching procedure with initial data at $x = x_{\text{in}}$.

Optimization Procedure

For optimization, one needs to choose a norm. The Mack energy norm[10]

$$E = \int_0^\infty \left[\rho_s (u^2 + v^2 + w^2) + \frac{\rho^2 T_s}{\gamma \rho_s M^2} + \frac{\theta^2 \rho_s}{\gamma(\gamma - 1) T_s M^2} \right] \mathrm{d}y \tag{4}$$

was adopted for the optimal analysis of compressible flow, within the scope of the parallel flow approximation.[5,6] Unlike the scaling (1), Eq. (4) was derived with v and w scaled with U_∞. The energy ratio was defined as $G^* = E_{\text{out}}/E_{\text{in}}$, where E_{in} and E_{out} correspond to the energy values (4) at initial and downstream coordinates x_{in} and x_{out}, respectively. The optimum energy ratio was the largest value of G^* obtained over the wave number space. As a result of the analysis, it was found that the optimal disturbances are steady streamwise vortices.

For the case of a nonparallel incompressible boundary layer, Luchini[8] suggested confining the optimization procedure within the scope of streamwise vortices as initial perturbations and observing only the streamwise velocity component at the downstream position. The procedure assumes an understanding of the physical mechanism leading to transient growth via the lift-up effect and significantly simplifies the optimization procedure. Andersson et al.[7] did not prescribe a specific initial perturbation, and they showed that their results agree with Luchini's results at high Reynolds numbers.

In the present work, we utilize Luchini's approach for the compressible boundary-layer flow, and we consider the optimization procedure in terms of the energy ratio as follows:

$$G = \frac{E_{\text{out}}}{E_{\text{in}}}, \qquad E_{\text{in}} = \int_0^\infty \left[\rho_s (v^2 + w^2) \right] \mathrm{d}y$$

$$E_{\text{out}} = \int_0^\infty \left[\rho_s u^2 + \frac{\rho^2 T_s}{\gamma \rho_s M^2} + \frac{\theta^2 \rho_s}{\gamma(\gamma - 1) T_s M^2} \right] \mathrm{d}y \tag{5}$$

In these equations, v and w are scaled with εU_∞ as defined in Eq. (1). Because the governing equations (2) do not contain the Reynolds number, the following results are Reynolds number independent. One can find, similar to the incompressible flow case,[7,8] that at high Reynolds numbers $G = G^*/Re$, that is, the ratio G^*/Re is independent of the Reynolds number. Employing the equation of state for the base flow and for the perturbations, one can find also the following expression for E_{out}:

$$E_{\text{out}} = \int_0^\infty \left[\rho_s u^2 + \frac{\theta^2}{(\gamma - 1) T_s^2 M^2} \right] \mathrm{d}y \tag{6}$$

The optimization procedure employs iterations of the solutions of the direct and adjoint problems as proposed in Refs. 7 and 8. Solution of the adjoint problem $\boldsymbol{g}$ satisfies (see Appendix B)

$$-\boldsymbol{A}^T \boldsymbol{g}_x = \left(\boldsymbol{D}^T \boldsymbol{g}_x\right)_y + \boldsymbol{B}_0^T \boldsymbol{g} - \left(\boldsymbol{B}_1^T \boldsymbol{g}\right)_y + \left(\boldsymbol{B}_2^T \boldsymbol{g}\right)_{yy} \tag{7}$$

and the following boundary conditions:

$$y = 0: g_2 = g_3 = g_4 = g_5 = 0$$

$$y \to \infty: g_1 + g_2 + 2V_s g_3 + g_5 + \tfrac{4}{3} g_{3y} = 0 \tag{8}$$

Equation (7) is parabolic, and one can solve it by means of an upstream marching procedure with initial data at $x = x_{\text{out}}$.

The modified version of the optimization algorithm from Ref. 7 will include temperature perturbations and the following steps:

1) Solve Eq. (3) with boundary conditions (2) and initial conditions

$$v(x_{\text{in}}, y), \qquad w(x_{\text{in}}, y) \neq 0$$
$$u(x_{\text{in}}, y) = 0, \qquad \theta(x_{\text{in}}, y) = 0 \tag{9}$$

The special form of the inflow profiles in Eq. (9) stems from that the optimal disturbances are associated with streamwise vortices in the shear flow. Therefore, v and w in the inflow will generate the transient growth due to the lift-up mechanism.

2) The adjoint equations (7) are solved upstream with boundary conditions (8) and initial data at $x = x_{\text{out}}$ as follows:

$$A^{11}(x_{\text{out}}, y) g_1(x_{\text{out}}, y) + A^{21}(x_{\text{out}}, y) g_2(x_{\text{out}}, y) + A^{51}(x_{\text{out}}, y) g_5(x_{\text{out}}, y) = \rho_s(x_{\text{out}}, y) u(x_{\text{out}}, y)$$

$$g_3 = (x_{\text{out}}, y) = g_4(x_{\text{out}}, y) = 0$$

$$A^{14}(x_{\text{out}}, y) g_1(x_{\text{out}}, y) + A^{24}(x_{\text{out}}, y) g_2(x_{\text{out}}, y) = \frac{\theta(x_{\text{out}}, y)}{(\gamma - 1)[T_s(x_{\text{out}}, y) M]^2} \tag{10}$$

where A^{ij} stands for the i, j element of matrix $\boldsymbol{A}$. Equations (10) originate from the conservation law [Eq. (B6) in Appendix B and derivation in Ref. 7] if one assumes that $v(x_{\text{out}}, y) = w(x_{\text{out}}, y) = 0$ in accordance with the concept of the optimal disturbances ending as a streaky structure.[7,8] Four equations (10) still can be satisfied by various choices of, for example, function $g_2(x_{\text{out}}, y)$. In the present implementation of the algorithm, we choose $g_2(x_{\text{out}}, y) = 0$.

3) Step 1 is repeated with initial data at $x = x_{\text{in}}$, found from the following equations originating from the conservation law:

$$v(x_{\text{in}}, y)\rho_s(x_{\text{in}}, y) = A^{32}(x_{\text{in}}, y)g_3(x_{\text{in}}, y)$$

$$w(x_{\text{in}}, y)\rho_s(x_{\text{in}}, y) = A^{43}(x_{\text{in}}, y)g_4(x_{\text{in}}, y)$$

$$u(x_{\text{in}}, y) = 0, \qquad \theta(x_{\text{in}}, y) = 0 \tag{11}$$

The iterations are carried out with normalization

$$E_{\text{in}} = \int_0^\infty \left[\rho_s(v^2 + w^2)\right] \mathrm{d}y = 1$$

Usually, three iterations are enough to provide accuracy of the energy ratio G within 1%.

Numerical Procedure

In the present work, we adopt the numerical procedure from Ref. 7 that was used for the analysis of optimal disturbances in a Blasius boundary layer.

Equation (3) is approximated in the streamwise direction with a fully implicit finite difference scheme of the second order (except for the first step)

$$\frac{3}{2}(\boldsymbol{Af})^{n+1} - 2(\boldsymbol{Af})^n + \frac{1}{2}(\boldsymbol{Af})^{n-1} = \frac{3}{2}\left(\boldsymbol{D}\frac{\partial \boldsymbol{f}}{\partial y}\right)^{n+1} - 2\left(\boldsymbol{D}\frac{\partial \boldsymbol{f}}{\partial y}\right)^n + \frac{1}{2}\left(\boldsymbol{D}\frac{\partial \boldsymbol{f}}{\partial y}\right)^{n-1} + \Delta x\left[(\boldsymbol{B}_0\boldsymbol{f})^{n+1} + \left(\boldsymbol{B}_1\frac{\partial \boldsymbol{f}}{\partial y}\right)^{n+1} + \left(\boldsymbol{B}_2\frac{\partial^2 \boldsymbol{f}}{\partial y^2}\right)^{n+1}\right], \qquad n = 1, \ldots, J-1 \tag{12}$$

$$(\boldsymbol{Af})^1 - (\boldsymbol{Af})^0 = \left(\boldsymbol{D}\frac{\partial \boldsymbol{f}}{\partial y}\right)^1 - 2\left(\boldsymbol{D}\frac{\partial \boldsymbol{f}}{\partial y}\right)^0 + \Delta x\left[(\boldsymbol{B}_0\boldsymbol{f})^1 + \left(\boldsymbol{B}_1\frac{\partial \boldsymbol{f}}{\partial y}\right)^1 + \left(\boldsymbol{B}_2\frac{\partial^2 \boldsymbol{f}}{\partial y^2}\right)^1\right] \tag{13}$$

where $\Delta x = 1/J$ is the step along the streamwise coordinate. At each streamwise coordinate x, we solve the one-dimensional boundary-value problem along the coordinate y using the spectral collocation method with Chebyshev polynomials. The Chebyshev interval was transformed to the domain $0 \le y \le y_{\max}$. The resulting linear algebraic system for the coefficients was solved using the routine DLSARG from the IMSL FORTRAN Library. After comparison of results with different $y_{\max}$, different steps along x, and different numbers of Chebyshev polynomials, N, the values $y_{\max} = 100$, $J = 100$, and $N = 100$ were chosen for the present analysis. At these parameters, our results were graphically indistinguishable from results obtained at $J = N = 200$. The same numerical scheme was applied for the discretization of Eq. (7).

Results

The main results of Refs. 5, 7, and 8 were repeated to validate the new model. To begin, we consider parallel boundary-layer flow as in Ref. 5. For this purpose, we chose $U_s(x, y) = U_s(x_{\text{out}}, y)$, $T_s(x, y) = T_s(x_{\text{out}}, y)$, and $V_s = 0$. Figure 1 shows a comparison of the optimal energy ratio vs x from Ref. 5 ($M = 0$) and the present model ($M = 0.02$) at $\beta = 0.45$. Figure 2 is a comparison of the results

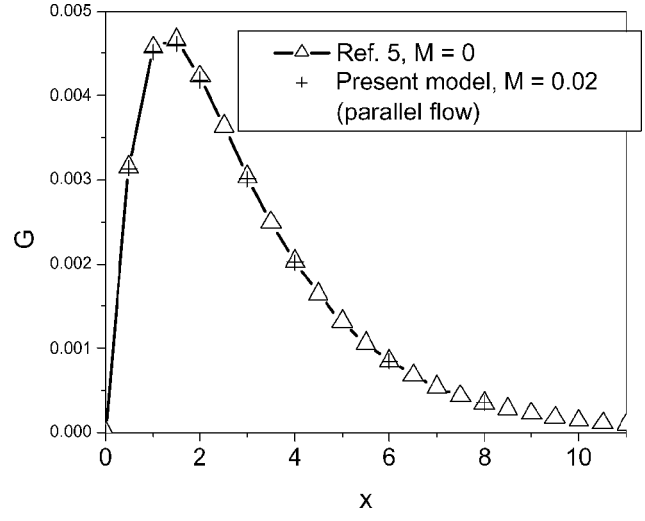

Fig. 1 Comparison of present model with Ref. 5 ($\beta = 0.45$).

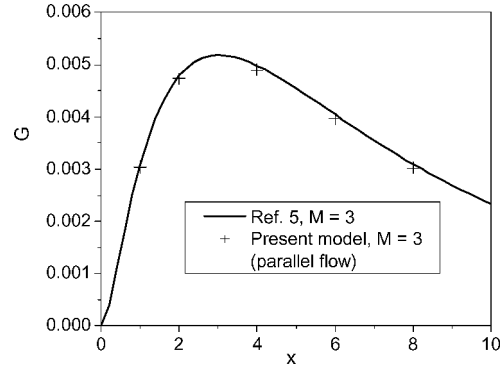

Fig. 2 Comparison of present model with Ref. 5 ($\beta = 0.2$).

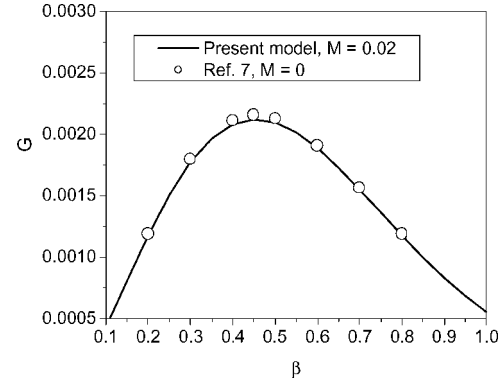

Fig. 3 Comparison of present model with Ref. 7; optimal energy vs wave number.

at $M = 3$ and adiabatic wall conditions. The slight discrepancy might be attributed to the different governing equations (linearized Navier–Stokes equations in Ref. 5 and linearized boundary-layer equations in the present model). The comparisons also serve as verification of our previous results,[5] inasmuch as we repeat them by an independent method. Note that the parallel flow model in Ref. 5 employed a completeness of the eigenfunction system. (The solution was spanned on a finite number of eigenmodes.) The comparisons in Figs. 1 and 2 actually demonstrate that the completeness theorem does work.

A comparison of the present model (nonparallel flow effects included) and the results of Ref. 7 for optimal energy growth vs spanwise wave number β is shown in Fig. 3. Figure 4 is a comparison of the results for the optimal energy ratio vs the downstream coordinate x. We also compare optimal velocity profiles $|v|$ and $|w|$

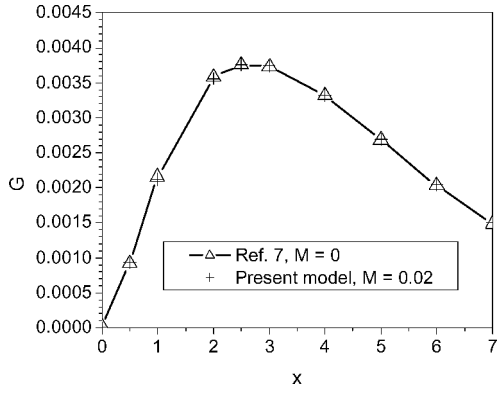

Fig. 4 Comparison of present model with Ref. 7 ($\beta = 0.45$); optimal energy vs coordinate x.

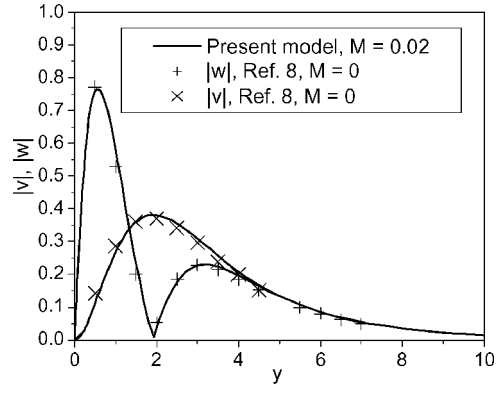

Fig. 5 Comparison of present model with Ref. 8 ($\beta = 0.45$); optimal input velocity profiles v and w.

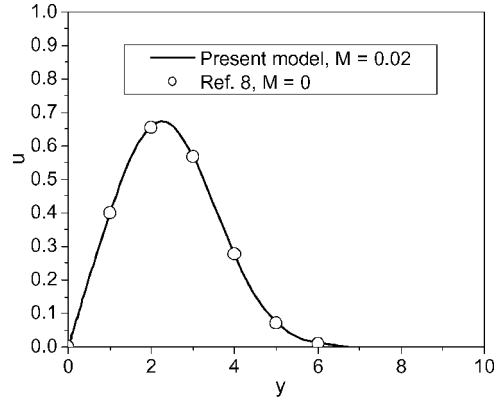

Fig. 6 Comparison of present model with Ref. 8 ($\beta = 0.45$); optimal output velocity profile u.

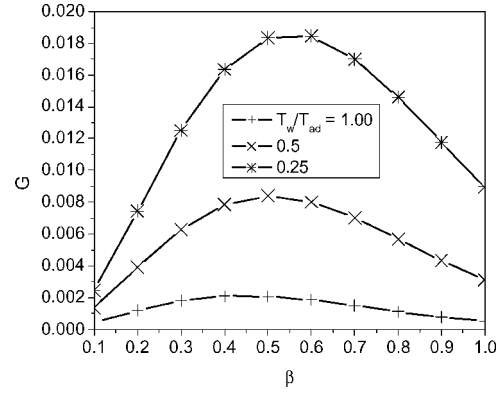

Fig. 7 Effect of wall temperature on the optimal energy growth ($M = 0.5, x_{in} = 0$, and $x_{out} = 1$).

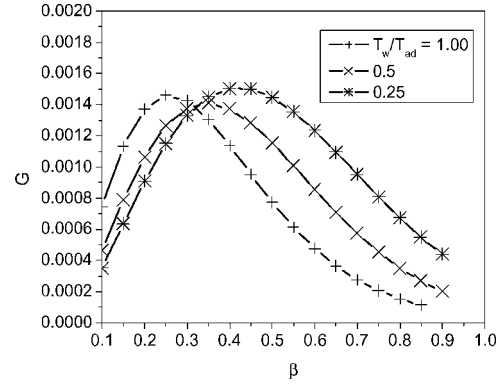

Fig. 8 Effect of wall temperature on the optimal energy growth ($M = 3.0, x_{in} = 0$, and $x_{out} = 1$).

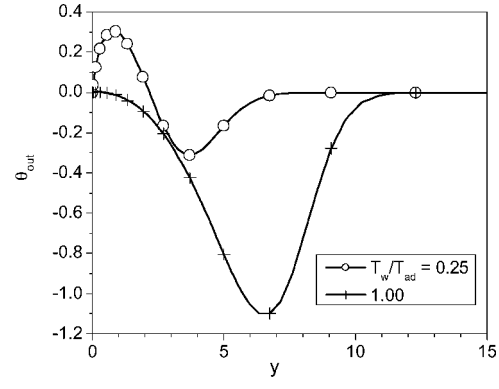

Fig. 9 Effect of wall temperature on the temperature streak growth ($M = 3.0, \beta = 0.35, x_{in} = 0$, and $x_{out} = 1$).

at $x = x_{in}$ and u at $x = x_{out}$ from Ref. 8 and the present model at $M = 0.02$ in Figs. 5 and 6. The agreement of results obtained in Refs. 7 and 8 with the results obtained including compressibility and nonparallel flow effects verifies the new model. Also, Figs. 3–6 demonstrate that the present theoretical model allows analysis of an incompressible flow using a small Mach number in the calculations.

Because the new model has been verified, we now consider results obtained in compressible boundary layers including nonparallel flow effects. Figures 7 and 8 demonstrate temperature effects on the optimal energy growth in subsonic ($M = 0.5$) and supersonic ($M = 3$) boundary layers. The results are qualitatively and quantitatively similar to those obtained in the parallel flow approximation.[5] The comparisons of the new results (Figs. 7 and 8) with results in Ref. 5 indicate that the nonparallel flow effects probably are not significant for estimates of transient growth. However, the parallel flow approximation, in addition to the discrepancies in the maximum of the energy growth and in its location downstream, does not answer how experimental and theoretical data can be compared on a length scale of order L.

The wall temperature effect on the velocity and temperature perturbations was not investigated in Ref. 5. Here, we present the new results including the nonparallel flow effects. Figures 9 and 10 show the temperature and streamwise velocity perturbations at $x_{out} = 1$. The corresponding optimal perturbations of v and w at $x_{in} = 0$ are demonstrated in Figs. 11 and 12, respectively. It is interesting that the optimal inputs corresponding to $T_w/T_{ad} = 0.25$ and 1.00 are almost the same, whereas the output profiles are strongly affected by the temperature factor.

Figure 13 demonstrates the effects of spanwise wave number and the initial coordinate $x = x_{in}$. There is an optimal wave number β and an optimal starting point, $x = x_{in}$ (The starting point effect was also found independently by Levin and Henningson[11] for incompressible

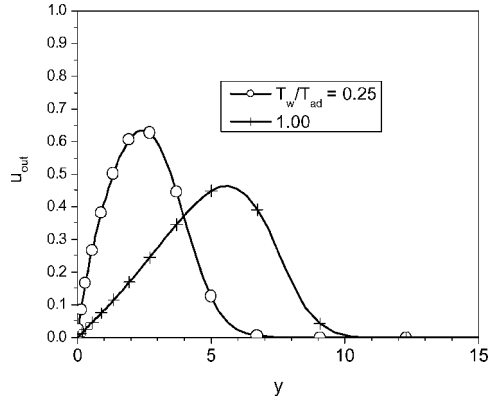

Fig. 10 Effect of wall temperature on the velocity streak growth ($M = 3.0$, $\beta = 0.35$, $x_{in} = 0$, and $x_{out} = 1$).

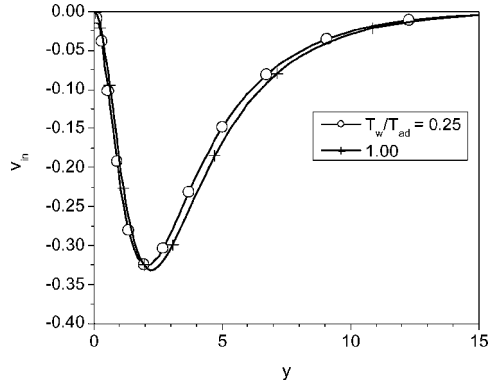

Fig. 11 Effect of wall temperature on the optimal input normal velocity growth ($M = 3.0$, $\beta = 0.35$, $x_{in} = 0$, and $x_{out} = 1$).

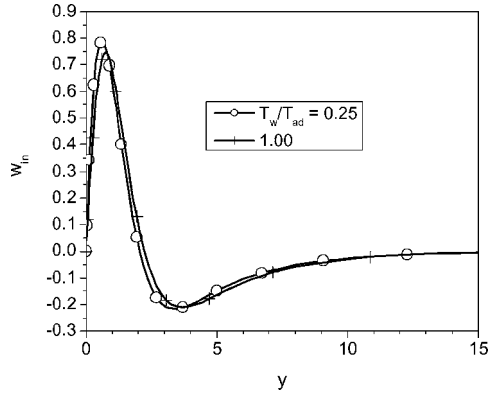

Fig. 12 Effect of wall temperature on the optimal input spanwise velocity growth ($M = 3.0$, $\beta = 0.35$, $x_{in} = 0$, and $x_{out} = 1$).

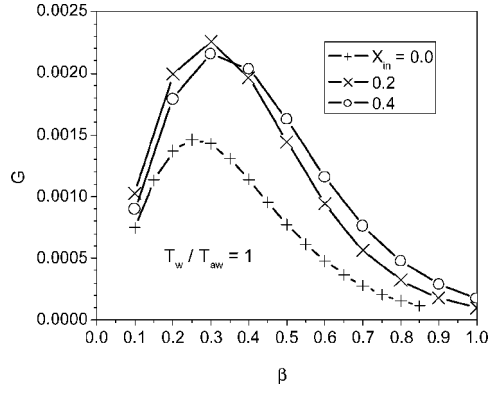

Fig. 13 Effect of starting point x_{in} and wave number on the optimal energy growth ($M = 3.0$).

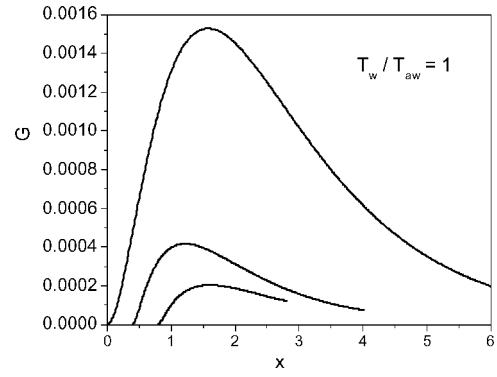

Fig. 14 Comparison of optimal and nonoptimal initial perturbations; velocity profiles v and w correspond to the optimal conditions at $x_{in} = 0$ and $x_{out} = 1$ ($M = 3.0$ and $\beta = 0.35$).

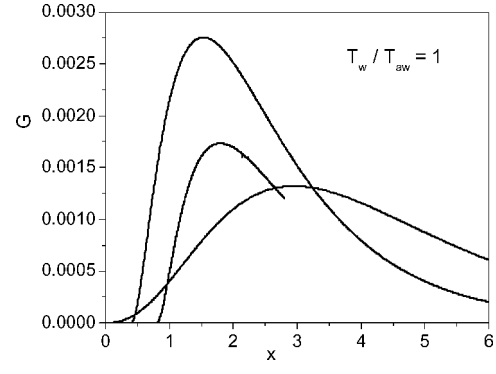

Fig. 15 Comparison of optimal and nonoptimal initial perturbations; velocity profiles v and w correspond to the optimal conditions at $x_{in} = 0.4$ and $x_{out} = 1$ ($M = 3.0$ and $\beta = 0.35$).

boundary layers.) The result means that if one would like to employ the transient growth mechanism by placing vortex generators on the wall, there is an optimal spacing in the spanwise direction and an optimal location from the leading edge.

One can expect that the initial velocity profiles in real experiments will not fit precisely the optimal perturbations. Therefore, it is interesting to compare downstream developments of optimal and nonoptimal disturbances. In Fig. 14, we use initial profiles of v and w corresponding to the optimal conditions at $x_{in} = 0$ and $x_{out} = 1$, applying them at $x_{in} = 0.4$ and $x_{in} = 0.8$. In Fig. 15, we compare results with $x_{in} = 0$, 0.4, and 0.8, when initial profiles correspond to optimal perturbations at $x_{in} = 0.4$ and $x_{out} = 1$. These results indicate that comparisons of theoretical predictions within the concept of the optimal perturbations with experimental data might be sensitive to a deviation of the perturbation profiles from the optimal ones.

Conclusions

The present model of optimal transient growth is an extension of the model in Ref. 8 to the case of compressible boundary layers. Comparisons with the new results (Figs. 7 and 8) with results of Ref. 5 obtained within the scope of the parallel flow approximation indicate qualitative and quantitative agreement. This means that the parallel flow theory can be used for estimation of the transient growth phenomenon in subsonic and supersonic boundary layers. However, the parallel flow approximation does not provide correct values for the maximum of the energy growth or for its location downstream. Also, the parallel flow model does not answer how experimental and theoretical data can be compared on a length scale of order L.

The optimal perturbations are associated with streamwise vortices, and their effect on the flow results in velocity and temperature streaks. The new results demonstrate that wall temperature may strongly affect the temperature profiles of the perturbations, whereas profiles of the optimal perturbations at the input might be close. The latter phenomenon is associated with the temperature redistribution

across the boundary layer due to the presence of the streamwise vortices.

In addition to the optimal spacing of the streamwise vortices, there is an optimal starting point x_{in}. This means that, if one wishes to employ the transient growth mechanism in tripping the boundary layer (for example, by a tiny vortex generator), it will be necessary to find the optimal spacing within the boundary layer and the optimal location from the leading edge.

In the present work, only examples of boundary layers over a flat plate have been considered. The effects of pressure gradient including nonparallel flow effects should be addressed in future research.

Appendix A: Nonzero Elements of the Matrices in Eq. (3)

The equations of state and scaling (1) lead to the following relationship between perturbations of density ρ and temperature θ:

$$\rho = -\theta / T_s^2$$

The normal velocity component of the base flow is scaled with εU_∞, and the corresponding function V_s has $\mathcal{O}(1)$. Viscosity μ_s is assumed to be a function of temperature, and μ_s' stands for the derivative $\mathrm{d}\mu_s/\mathrm{d}T_s$.

Transformations of the linearized equations lead to the following matrix elements.

The continuity equation:

$$A^{11} = \rho_s, \qquad A^{14} = -\rho_s^2 U_s$$

$$B_0^{12} = -\frac{\partial \rho_s}{\partial y}, \qquad B_0^{13} = -\beta \rho_s, \qquad B_0^{14} = \frac{\partial}{\partial y}\left(\rho_s^2 V_s\right)$$

$$B_1^{12} = -\rho_s, \qquad B_1^{14} = \rho_s^2 V_s$$

The x-momentum equation:

$$A^{21} = 2\rho_s U_s, \qquad A^{24} = -(\rho_s U_s)^2, \qquad B_0^{21} = -\frac{\partial \rho_s V_s}{\partial y} - \mu_s \beta^2$$

$$B_0^{22} = -\frac{\partial \rho_s U_s}{\partial y}, \qquad B_0^{23} = -\beta \rho_s U_s$$

$$B_0^{24} = \frac{\partial\left(\rho_s^2 V_s U_s\right)}{\partial y} + \frac{\partial}{\partial y}\left[\mu_s' \frac{\partial U_s}{\partial y}\right], \qquad B_1^{21} = \frac{\partial \mu_s}{\partial y} - \rho_s V_s$$

$$B_1^{22} = -\rho_s U_s, \qquad B_1^{24} = \rho_s^2 V_s U_s + \mu_s' \frac{\partial U_s}{\partial y}, \qquad B_2^{21} = \mu_s$$

The y-momentum equation:

$$A^{31} = \rho_s V_s + \frac{2}{3}\frac{\partial \mu_s}{\partial y}, \qquad A^{32} = \rho_s U_s$$

$$A^{34} = -\rho_s^2 V_s U_s - \mu_s' \frac{\partial U_s}{\partial y}, \qquad B_0^{31} = \frac{2}{3}\frac{\partial^2 \mu_s}{\partial y \partial x}$$

$$B_0^{32} = -2\frac{\partial \rho_s V_s}{\partial y} - \beta^2 \mu_s, \qquad B_0^{33} = -\beta \rho_s V_s - \frac{2\beta}{3}\frac{\partial \mu_s}{\partial y}$$

$$B_0^{34} = 2\rho_s^2 V_s \frac{\partial V_s}{\partial y} + \frac{\partial \mu_s'}{\partial y}\left[\frac{4}{3}\frac{\partial V_s}{\partial y} - \frac{2}{3}\frac{\partial U_s}{\partial x}\right] + \mu_s' \frac{\partial}{\partial y}\left[\frac{4}{3}\frac{\partial V_s}{\partial y} - \frac{2}{3}\frac{\partial U_s}{\partial x}\right] + V_s^2 \frac{\partial \rho_s^2}{\partial y}$$

$$B_1^{31} = \frac{1}{3}\frac{\partial \mu_s}{\partial x}, \qquad B_1^{32} = -2\rho_s V_s + \frac{4}{3}\frac{\partial \mu_s}{\partial y}, \qquad B_1^{33} = \frac{\beta \mu_s}{3}$$

$$B_1^{34} = \mu_s', \left[\frac{4}{3}\frac{\partial V_s}{\partial y} - \frac{2}{3}\frac{\partial U_s}{\partial x}\right] + (\rho_s V_s)^2, \qquad B_1^{35} = -1$$

$$B_2^{32} = \frac{4\mu_s}{3}, \qquad D^{31} = \frac{\mu_s}{3}$$

The z-momentum equation:

$$A^{43} = \rho_s U_s, \qquad A^{44} = \frac{\mu_s \beta U_s}{3T_s}, \qquad B_0^{41} = \frac{\beta \mu_s}{3\rho_s}\frac{\partial \rho_s}{\partial x} - \beta \frac{\partial \mu_s}{\partial x}$$

$$B_0^{42} = \frac{\beta \mu_s}{3\rho_s}\frac{\partial \rho_s}{\partial y} - \beta \frac{\partial \mu_s}{\partial y} \qquad B_0^{43} = -\beta^2 \mu_s - \frac{\partial \rho_s V_s}{\partial y}$$

$$B_0^{44} = \rho_s^2 U_s \frac{\partial}{\partial x}\left[\frac{\beta \mu_s}{3\rho_s}\right] + \frac{2\beta}{3}\left(\frac{\partial U_s}{\partial x} + \frac{\partial V_s}{\partial y}\right)\mu_s' - \frac{\beta \mu_s}{3\rho_s}\frac{\partial\left(\rho_s^2 V_s\right)}{\partial y}$$

$$B_0^{45} = \beta, \qquad B_1^{43} = -\rho_s V_s + \frac{\partial \mu_s}{\partial y}$$

$$B_1^{44} = -\frac{\beta \mu_s V_s}{3T_s}, \qquad B_2^{43} = \mu_s$$

The energy equation:

$$A^{51} = 1, \qquad B_0^{53} = -\beta$$

$$B_0^{54} = \mu_s'(\gamma - 1)M^2\left(\frac{\partial U_s}{\partial y}\right)^2 - \frac{\beta^2 \mu_s}{Pr} + \frac{1}{Pr}\frac{\partial}{\partial y}\left(\mu_s' \frac{\partial T_s}{\partial y}\right)$$

$$B_1^{51} = 2(\gamma - 1)M^2 \mu_s \frac{\partial U_s}{\partial y}, \qquad B_1^{52} = -1$$

$$B_1^{54} = \frac{2}{Pr}\frac{\partial \mu_s}{\partial y}, \qquad B_2^{54} = \frac{\mu_s}{Pr}$$

Appendix B: Derivation of the Adjoint Equation

Integration of the scalar product of vector $\boldsymbol{g}$ and Eq. (3) over the domain $(x_{in}, x_{out}) \times (0, y_{max})$ leads to the following equation:

$$0 = \int_0^{y_{max}} \int_{x_{in}}^{x_{out}} \boldsymbol{g}^T \left[(A\boldsymbol{f})_x - (D\boldsymbol{f}_y)_x - B_0 \boldsymbol{f} - B_1 \boldsymbol{f}_y - B_2 \boldsymbol{f}_{yy}\right] \mathrm{d}x\, \mathrm{d}y$$

$$= \int_0^{y_{max}} \int_{x_{in}}^{x_{out}} \boldsymbol{f}^T \left[-A^T \boldsymbol{g}_x - \left(D^T \boldsymbol{g}_x\right)_y - B_0^T \boldsymbol{g} + \left(B_1^T \boldsymbol{g}\right)_y - \left(B_2^T \boldsymbol{g}\right)_{yy}\right] \mathrm{d}y\, \mathrm{d}x + \int_0^{y_{max}} \boldsymbol{f}^T(x_{out}) A^T(x_{out}) \boldsymbol{g}(x_{out})\, \mathrm{d}y$$

$$- \int_0^{y_{max}} \boldsymbol{f}_y^T(x_{out}) D^T(x_{out}) \boldsymbol{g}(x_{out})\, \mathrm{d}y - \int_0^{y_{max}} \boldsymbol{f}^T(x_{in}) A^T(x_{in}) \boldsymbol{g}(x_{in})\, \mathrm{d}y + \int_0^{y_{max}} \boldsymbol{f}_y^T(x_{in}) D^T(x_{in}) \boldsymbol{g}(x_{in})\, \mathrm{d}y$$

$$- \int_{x_{in}}^{x_{out}} \left[\boldsymbol{f}^T B_1^T \boldsymbol{g} + \boldsymbol{f}_y^T B_2^T \boldsymbol{g} - \boldsymbol{f}^T \left(B_2^T \boldsymbol{g}\right)_y\right] \mathrm{d}x \Big|_{y=0}^{y=y_{max}} \qquad \text{(B1)}$$

To satisfy Eq. (B1), we demand that $\boldsymbol{g}$ satisfies the adjoint equation

$$-\boldsymbol{A}^T\boldsymbol{g}_x = \left(\boldsymbol{D}^T\boldsymbol{g}_x\right)_y + \boldsymbol{B}_0^T\boldsymbol{g} - \left(\boldsymbol{B}_1^T\boldsymbol{g}\right)_y + \left(\boldsymbol{B}_2^T\boldsymbol{g}\right)_{yy} \tag{B2}$$

This equation provides nullification that the first term on the right-hand side of Eq. (B1) is equal to zero. The next step is to formulate the boundary conditions at $y=0$ and $y=y_{\max}$, leading to the last term in Eq. (B1) being equal to zero. Consideration of this term at $y=0$ together with the boundary conditions (2) leads to the following boundary conditions for the adjoint:

$$y=0\text{: } g_2 = g_3 = g_4 = g_5 = 0 \tag{B3}$$

Boundary conditions for Eq. (B2) at $y=y_{\max}$ stem from consideration of the same term and the boundary conditions (2) at $y=y_{\max}$. There are a few more terms that should be addressed. As the result of a finite value for $v(x, y_{\max})$, one can arrive at the following boundary condition for Eq. (B2):

$$y\to y_{\max}\text{: } g_1 + g_2 + 2V_s g_3 + g_5 + \tfrac{4}{3}g_{3y} = 0 \tag{B4}$$

There are also other terms having u_y, v_y, w_y, and θ_y as coefficients. In the case of $y_{\max}\to\infty$, the derivatives must tend to zero, and therefore, there are no additional boundary conditions for Eq. (B2). The boundary conditions (B3) and (B4) are similar to the boundary conditions in Ref. 8 except for the additional condition on the wall. In all cases, for numerical implementation, the boundary conditions at $y=0$ and $y=y_{\max}$ are supplemented by equations from system (3) at $y=0$ and $y=y_{\max}$ to provide five equations at both ends of the interval $[0, y_{\max}]$.

Finally, Eq. (B1) leads to the following conservation law:

$$\begin{aligned}\int_0^{y_{\max}} &\boldsymbol{f}^T(x_{\text{out}})\boldsymbol{A}^T(x_{\text{out}})\boldsymbol{g}(x_{\text{out}})\,\mathrm{d}y \\ &- \int_0^{y_{\max}} \boldsymbol{f}_y^T(x_{\text{out}})\boldsymbol{D}^T(x_{\text{out}})\boldsymbol{g}(x_{\text{out}})\,\mathrm{d}y \\ &= \int_0^{y_{\max}} \boldsymbol{f}^T(x_{\text{in}})\boldsymbol{A}^T(x_{\text{in}})\boldsymbol{g}(x_{\text{in}})\,\mathrm{d}y \\ &- \int_0^{y_{\max}} \boldsymbol{f}_y^T(x_{\text{in}})\boldsymbol{D}^T(x_{\text{in}})\boldsymbol{g}(x_{\text{in}})\,\mathrm{d}y\end{aligned} \tag{B5}$$

Because the iteration procedure (9–11) employs $u(x_{\text{in}})=0$ and $g_3(x_{\text{out}})=0$, the terms associated with matrix $\boldsymbol{D}$ in Eq. (B5) are equal to zero, and the conservation law has the same form as in the case for incompressible flow,[7]

$$\int_0^{y_{\max}} \boldsymbol{f}^T(x_{\text{out}})\boldsymbol{A}^T(x_{\text{out}})\boldsymbol{g}(x_{\text{out}})\,\mathrm{d}y = \int_0^{y_{\max}} \boldsymbol{f}^T(x_{\text{in}})\boldsymbol{A}^T(x_{\text{in}})\boldsymbol{g}(x_{\text{in}})\,\mathrm{d}y \tag{B6}$$

One can follow the analysis of Ref. 7 to show the consistency of the iteration scheme (9–11) with Eq. (B6).

Acknowledgment

This work is supported by the U.S. Air Force Office of Scientific Research.

References

[1]Reshotko, E., "Transient Growth: A Factor in Bypass Transition," *Physics of Fluids*, Vol. 13, 2001, pp. 1067–1075.

[2]Schmid, P. J., and Henningson, D. S., *Stability and Transition in Shear Fflows*, Springer, New York, 2001, pp. 56, 57, 99–103.

[3]Reshotko, E., and Tumin, A., "The Blunt Body Paradox—A Case for Transient Growth," *Laminar–Turbulent Transition*, edited by H. F. Fasel and W. S. Saric, Springer, New York, 2001, pp. 403–408.

[4]Reshotko, E., and Tumin, A., "Spatial Theory of Optimal Disturbances in a Circular Pipe Flow," *Physics of Fluids*, Vol. 13, 2001, pp. 991–996.

[5]Tumin, A., and Reshotko, E., "Spatial Theory of Optimal Disturbances in Boundary Layers," *Physics of Fluids*, Vol. 13, 2001, pp. 2097–2104.

[6]Hanifi, A., Schmid, P. J., and Henningson, D. S., "Transient Growth in Compressible Boundary Layer Flow," *Physics of Fluids*, Vol. 8, 1996, pp. 51–65.

[7]Andersson, P., Berggren, M., and Henningson, D. S., "Optimal Disturbances and Bypass Transition in Boundary Layers," *Physics of Fluids*, Vol. 11, 1999, pp. 134–150.

[8]Luchini, P., "Reynolds Number Independent Instability of the Boundary Layer over a Flat Surface, Part 2: Optimal Perturbations," *Journal of Fluid Mechanics*, Vol. 404, 2000, pp. 289–309.

[9]El-Hady, N. M., and Verma, A. K., "Instability of Compressible Boundary Layers Along Curved Walls with Suction and Cooling," *AIAA Journal*, Vol. 22, 1983, pp. 206–213.

[10]Mack, L. M., "Boundary Layer Stability Theory," Jet Propulsion Lab., JPL Rept. 900-277, California Inst. of Technology, Pasadena, CA, Nov. 1969.

[11]Levin, O., and Henningson, D., "Algebraic vs. Exponential Growth," *Bulletin of the American Physical Society*, Vol. 47, No. 10, 2002, p. 136.

A. Plotkin
Associate Editor